

phase in our system, this ripple structure would provide a reasonable explanation of the intermediate structure observed in Fig. 2B. The ripple phase has been observed in many lipid systems (24) and can include macroripples with wavelengths of ~100 nm (25). The slow neutralization strategy is necessary to leave enough time for the soft layer containing the hexagonal phase to bend.

19. It has been reported by Z. Luan *et al.* [*J. Chem. Soc. Faraday Trans.* **91**, 2955 (1995)] that the crystal size of MCM-41 is reduced after incorporation of alumi-

num into the structure. In our case, this is reflected in shorter and thinner tubules when aluminum is incorporated into the framework.

20. H. P. Lin, S. Cheng, C.-Y. Mou, unpublished results.
21. L. H. Burekle, in *Introduction to Marine Micropaleontology*, B. U. Haq and A. Boersma, Eds. (Elsevier, New York, 1978), pp. 245–266.
22. The difference in pH between experimental conditions and the naturally occurring state of diatoms should be noted.
23. S. Mann, *J. Mater. Chem.* **5**, 935 (1995).

24. J. A. N. Zasadzinski, J. Schneir, J. Gurley, V. Ellings, P. K. Hansma, *Science* **239**, 1013 (1988); D. C. Wack and W. W. Webb, *Phys. Rev. Lett.* **61**, 1210 (1988).
25. R. E. Brown, W. H. Anderson, V. S. Kulkarni, *Biophys. J.* **68**, 1396 (1995).
26. Supported by the National Science Council of Taiwan (NSC 85-2113-M-002-032cc). We thank S. Cheng and M.-P. Chen for valuable discussions.

2 April 1996; accepted 13 June 1996

Oil-Water Interface Templating of Mesoporous Macroscale Structures

S. Schacht, Q. Huo, I. G. Voigt-Martin, G. D. Stucky, F. Schüth*

Ordered mesostructured porous silicas that are also macroscopically structured were created by control of the interface on two different length scales simultaneously. Micellar arrays controlled the nanometer-scale assembly, and at the static boundary between an aqueous phase and an organic phase, control was achieved on the micrometer to centimeter scale. Acid-prepared mesostructures of silica were made with the *p6*, *Pm3n*, and the *P6₃/mmc* structures in the form of porous fibers 50 to 1000 micrometers in length, hollow spheres with diameters of 1 to 100 micrometers, and thin sheets up to 10 centimeters in diameter and about 10 to 500 micrometers in thickness. These results might have implications for technical applications, such as slow drug-release systems or membranes, and in biomineralization, where many processes are also interface-controlled.

As noted by Israelachvili (1), microemulsions and emulsions occupy a special place in the hierarchy of structures, in that their formation involves long-range forces with an energy of assembly, including shape fluctuations and interaggregate interactions, approximately equal to the thermal energy kT . Hydrodynamic long-range forces can therefore be used to define emulsion morphology and the configuration of the emulsion oil-water interface. If an oil-in-water interface is used as an inorganic growth medium with the growth direction into the aqueous phase, morphological control of the resulting inorganic-organic composite assembly can be achieved at micrometer and longer length scales.

At a somewhat smaller length scale, mesoscale patterned silica-organic composite phases with organic domain dimensions of up to 0.01 μm and periodic repeats of as much as 0.02 μm (2) can now be created in a variety of two- and three-dimensional (2D and 3D) periodic arrays (3–7). These ordered organic-inorganic composite precursors of porous oxide structures form in a

cooperative way under the influence of surfactants (4–10), with the nanophase dimensions and the overall 3D periodic geometries determined primarily by the surfactant molecular shape and geometry.

We combined long-range oil-in-water emulsion and oil-water interface physics with the shorter range cooperative assembly of silica and surfactants at the oil-water interface to create ordered composite mesostructured phases that are also macroscopically structured. The organic “oil” and surfactant can be removed from the silica phase to give mesoporous structures. Here the emulsion or the interface, or both, exerts morphological control during the formation of the inorganic gel or crystals.

With self-assembly energies approaching kT , emulsions are often close to the limit of stability. Oil-in-water emulsions are stabilized by short-range (10^{-7} m) and relatively weak van der Waals interactions between the hydrophobic tails of amphiphilic surfactants and the emulsion organic phase. The M41S silicate mesostructures first described by the Mobil group were synthesized with surfactants under alkaline conditions (pH 11 to 12). Under these basic conditions, composite formation is dominated by strong, direct interactions between positively charged surfactant (S^+) with negative inorganic silica solution species (I^-) and the consequent intermolecular interactions among the resulting molecular ion pairs

(S^+I^-) (9). This interaction is energetically disadvantageous for the creation of silica composite macroscale structures by the process of “coating” surfactant molecules that are weakly coordinated to an organic surface through van der Waals interactions because if the surfactant molecules are abstracted from the organic media, macroscopic control of the product by the organic phase is lost.

An alternative synthetic approach is to use acid-prepared mesostructures (APMs) synthesized from very acidic solutions below the pH of the isoelectric point of silica (5). Under these conditions, halide ions (X^-) mediate the interaction between the surfactant and positively charged inorganic species ($S^+X^-I^+$) through weak hydrogen bonding forces so that the identity of the surfactant-coated organic surface is maintained (11). Silica mesostructured phases synthesized in this fashion have different composition, pore structure, and absorption properties compared with samples synthesized under alkaline conditions (12).

With this in mind, we exploited the biphasic control in the synthesis of APMs on two different length scales simultaneously: synthesis at one scale forms the surfactant inorganic nanocomposite, and the other controls the secondary particle morphology on the micrometer to centimeter scale, with the large-scale control being similar to the approach of Walsh *et al.* (13). We used auxiliary organics to create an oil-in-water emulsion. In the acidic synthesis, tetraethoxysilane (TEOS) was the silica source. It hydrolyzes under acidic conditions and then condenses to form the APM. If auxiliary organics, such as *n*-hexane, benzene, toluene, mesitylene, or others are used, the oil-in-water emulsion is formed where the TEOS is dissolved in the oil droplets that are surrounded by an acidic aqueous solution with surfactant concentrated in the interface. The TEOS is hydrolyzed just at the oil-water interface, and there forms the mesostructure, which reflects on a larger length scale the size and shape of the oil spheres because the inorganic material solidifies around them.

A typical synthesis was carried out as follows: The surfactant [4.74 g of $C_{16}H_{33}N(CH_3)_3Br$ or similar molar amounts of

S. Schacht and F. Schüth, Institut für Anorganische Chemie, Johann Wolfgang Goethe Universität Frankfurt, Marie Curie Straße 11, 60439 Frankfurt, Germany.

Q. Huo and G. D. Stucky, Department of Chemistry, University of California, Santa Barbara, CA 93106, USA.
I. G. Voigt-Martin, Institut für Physikalische Chemie, Johannes Gutenberg-Universität Mainz, Welderweg 11, 55099 Mainz, Germany.

*To whom correspondence should be addressed.

other surfactants] was dissolved in 250 ml of water. Then 34 ml of aqueous HCl (37 weight %) was added. To this solution a mixture of 7 g of the auxiliary organic (typically mesitylene) and 4 g of TEOS was added slowly over 30 min while stirring at room temperature. During this time an emulsion forms. Stirring is one mechanism for controlling emulsion properties through modification of long-range hydrodynamic forces and is crucial in the formation of the secondary morphology (14, 15) (Fig. 1). Under slow stirring, predominantly fiber-type morphologies are observed. The rope-like fibers consist of several smaller strands that intertwine during the process of silica condensation.

However, the first transmission electron micrographs (TEMs) and preliminary data from pulsed-field gradient nuclear magnetic resonance experiments (16) suggest that the channels preferentially orient parallel to the

fiber axis. With increasing stirring rate, more and more spherulike particles are formed until the fiber morphology disappears completely. The size of the spherical particles decreases with increasing stirring rate.

By carefully tuning the synthesis conditions, especially at low concentrations of TEOS, we prepared samples that consisted entirely of rather spherical particles with a relatively narrow size distribution (Fig. 1B). However, the particles had agglomerated into lumps. This aggregation was probably due to condensation of uncondensed surface groups of different spheres when they came into contact with each other in a later stage of the synthesis. This agglomeration can be avoided if the synthesis mixture is diluted, after the spheres have developed, by pouring the mixture (300 ml) into 2 liters of water and then slowly filtering the resulting suspension. Using such a procedure, we produced almost exclusively isolated particles; however, the total solids yield was only about 20%.

These particles are in fact hollow after the organic phase has been removed. Particles from the same batch as depicted in Fig. 1B were treated with a spatula on the sample holder of the scanning electron microscope

(SEM). Most of the particles were crushed, and the void inside of each particle was open to the eye (Fig. 2A). The SEM image of a sample that consisted of thin-walled larger spheres, most of which popped open during the drying and calcination steps after preparation or during introduction into the high vacuum of the SEM, is shown in Fig. 2B.

These samples, consisting entirely of such spherical particles, have all of the features of the regular APMs (17). For example, Fig. 3 shows the x-ray diffraction pattern of a phase exhibiting three peaks that can be indexed in a $p6m$ hexagonal unit cell. The sorption isotherm for such APMs is different from that of MCM-41 synthesized from alkaline media (12). The capillary condensation step is not as steep, a high BET (Brunauer-Emmett-Teller) surface area is calculated (which suggests microporosity), and the step in the isotherm is normally shifted to lower values of normalized pressure p/p_0 , which corresponds to a secondary micropore filling process rather than real capillary condensation. Another difference compared with MCM-41 is observed in thermogravimetric experiments. The samples lose about 60% of their weight between 200° and 600°C, first in an endothermic and then in two distinct exothermic processes. A weight loss of ~4.5% before this stage is probably due to water. The unusually high weight loss can be attributed to the air-dried samples having

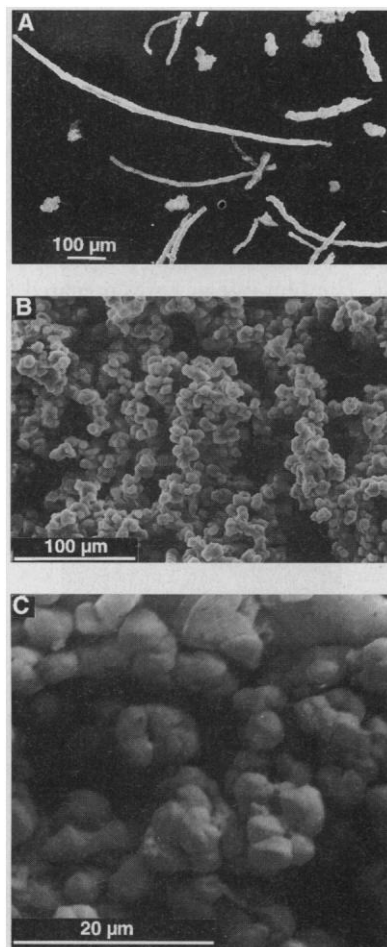


Fig. 1. Dependence of the morphology of the APM materials on the stirring rate, as seen with a SEM. At low stirring rates [(A) 120 revolutions per minute (rpm)], fibrous particles are formed, whereas at higher rates [(B) 220 rpm and (C) 400 rpm], the particles are spherical. The sizes of the spheres decrease with increasing stirring speed. The particles in (B) were made under dilute conditions.

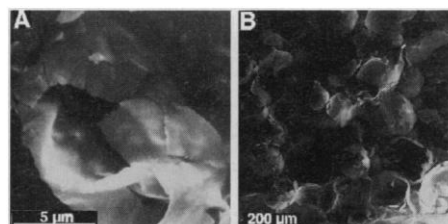


Fig. 2. (A) Particles from Fig. 1B after crushing with a spatula. (B) Shell fragments of larger particles. The larger spheres are relatively unstable mechanically and collapse either during processing after synthesis or during introduction into the high vacuum of the sample chamber of the SEM.

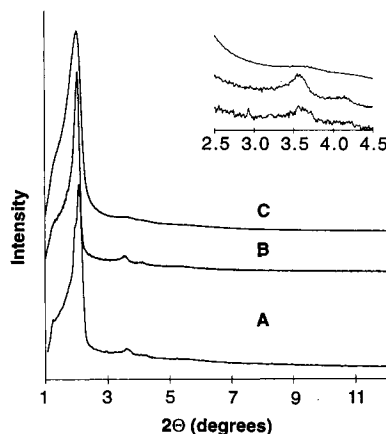


Fig. 3. X-ray diffraction pattern of the sample from Fig. 2 in the (A) as-made, (B) dried (at 90°C), and (C) calcined (at 500°C) form. (Inset) Three peaks corresponding to a $p6$ structure can be discerned.

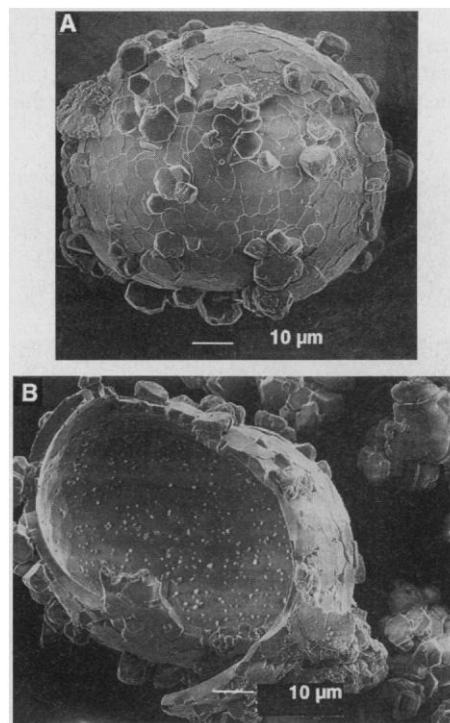


Fig. 4. SEM images of (A) a hollow sphere consisting of the generated intergrowth of platelike particles with the $P6_3/mmc$ structure and (B) the same sphere after being crushed.

appreciable amounts of organics occluded in the internal voids of the particles, in addition to the surfactant molecules in the pores, that volatilize during the thermogravimetric experiment.

These structures can also be synthesized as $P6_3/mmc$ and $Pm3n$ phases. For such preparations, large head-group surfactants must be used as described by Huo *et al.* (6). Dissolving 1 g of gemini surfactant (18-6-1) in 56 g of 1.5 M HCl and then adding 4 g of TEOS in 1.2 g of mesitylene over 40 min while stirring at room temperature results in the formation of a white, solid product after 3 hours of stirring. This product contains hollow spheres (Fig. 4) $\sim 50 \mu\text{m}$ in diameter and consists of intergrown platelike particles that are characteristic of the $P6_3/mmc$ phase. The diffraction pattern is identical to reported patterns for the $P6_3/mmc$ phase (lattice constants $a = 5.02 \text{ nm}$, $c = 8.84 \text{ nm}$, and $c/a = 1.63$ after calcination at 500°C).

The formation of the particles can actually be followed in real time under an optical microscope. If a liquid sample is taken from the reaction mixture $\sim 15 \text{ min}$ after the complete addition of the TEOS and immediately placed on a glass slide and viewed through an optical microscope, one can detect oil droplets that are in the process of being covered with a silica skin. A series of micrographs taken of an individual sphere during the formation of the silica skin (Fig. 5) show that the oil droplet is first completely transparent and then becomes gradually covered by a skin that somewhat scatters light. The situation in the optical microscope is certainly not identical to the

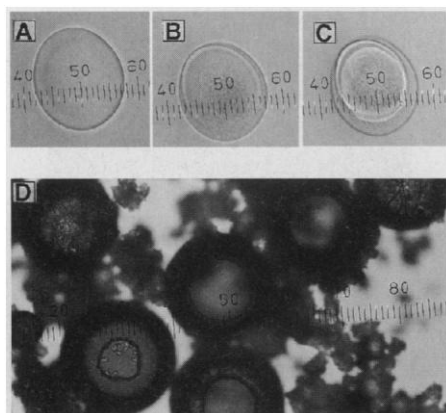


Fig. 5. Evolution of the spherical particles as seen in an optical microscope. Fifteen minutes after all of the TEOS was added, a drop of the reaction mixture was placed on a slide and a sphere was selected. (A) The pure mesitylene sphere. (B) After 10 s, a first APM layer formed. (C) After $\sim 30 \text{ s}$, this layer grew as more TEOS was hydrolyzed at the interface. (D) A growing sphere (left bottom) and a completely formed sphere (left top). The spheres in the center are partially closed.

situation in the stirred bulk solution, but we believe that a similar process is occurring there to form the hollow APM particles.

We suggest a model for the formation of such materials according to the process sketched in Fig. 6: Addition of TEOS dissolved in an organic solvent to the acidic solution containing the surfactant while stirring creates an oil-in-water emulsion. Surfactant is enriched at the oil-water interface and contributes to the stabilization of this emulsion. Then TEOS is hydrolyzed under acidic conditions at the interface, and there forms the mesostructure under the influence of the surfactant. There are TEM indications that the major parts of the APM pores are oriented radially in the shell of the hollow particles.

After the successful preparation of the hollow-sphere materials, we used the two-level biphasic control on a larger scale, to fabricate self-supporting membranes at a static interface between an aqueous and an organic phase. The chemical compositions of the two phases were the same as those used in the preparation of the sphere morphology. The addition of the organic phase to the aqueous phase, however, was carried out very carefully in a crystallization dish to top the aqueous phase with the organic phase with as little mixing as possible. Alternatively, tribromomethane was used to

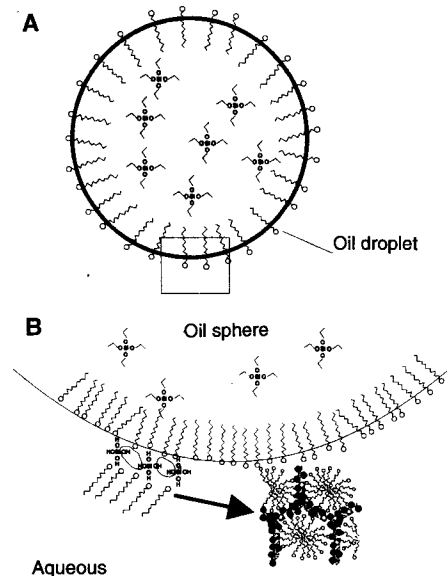


Fig. 6. Schematic drawing of the suggested formation process of the spheres. (A) The mesitylene drops in the mesitylene-aqueous HCl emulsion contain the dissolved TEOS; the emulsion is stabilized by the surfactant in the interface. (B) At the interface [area in (A) expanded], TEOS is hydrolyzed and solidifies there to an APM under the influence of the surfactant at the interface, mediated by chloride ions (not shown). The morphology of the final product is more or less molded on the original mesitylene droplet.

reverse the order of the aqueous and the organic phases. About 5 min after addition of the organic phase, the formation of a thin film, which is at first patchy but later gives a coherent solid sheet, could be observed with the naked eye. The largest diameter for such films achieved so far is $\sim 10 \text{ cm}$ with a thickness of $\sim 0.5 \mu\text{m}$. The film quality varied, depending on the conditions used, such as the concentration of TEOS in the organic phase and the organic solvent. For the TEM, a piece of a film formed at a decane-water interface auxiliary was removed from the interface with a copper-carbon grid and calcined at 300°C . The TEM shows that pores are predominantly hexagonally ordered and perpendicular to the film; the rest are probably less ordered but also appear to be perpendicular to the film (Fig. 7). The films can be isolated by evaporating the solvent and directly drying them in the crystallization dish, or even with pincers.

Usually only one to two low-angle peaks can be detected in the film. A SEM image (Fig. 8) shows thin sheets on the copper-carbon grid of the TEM in Fig. 7. The cracks are formed by handling of the thin sheets. Thicker films consist of agglomerated particles but are relatively crack-free. Whether these films have pores only in the size range of APM materials or also have larger pores is not clear. The film in Fig. 8 was prepared at a higher TEOS concentration than was the

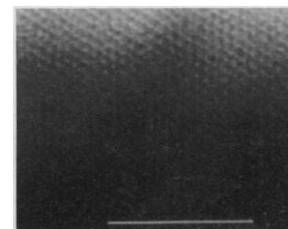


Fig. 7. TEM of an APM film with decane as organic auxiliary. This film was removed with a copper-carbon grid and calcined at 300°C . The pores are predominantly hexagonally ordered and oriented perpendicular to the film. Scale bar, 50 nm. Tilting experiments proved that the hexagonal structures are not a Moiré pattern.

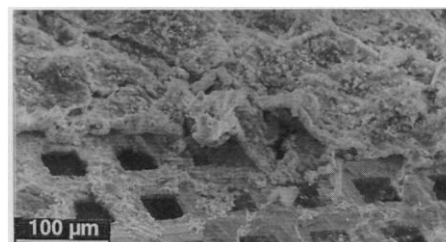


Fig. 8. SEM image of the sheets on the copper-carbon grid in Fig. 7.

film in Fig. 7, to grow it thicker and make it easier to handle.

These materials may have technological as well as fundamental implications. The hollow spheres, for instance, could be used as controlled drug-delivery systems. The membranes might be developed further for separation processes, where nanometer-scale pores are needed. From a more fundamental point of view, the process described here for structuring inorganic material might in a modified form be applicable to the formation of structured inorganic segments in living organisms. It is by now almost certain that interfaces play a crucial role in biomineralization (18), and the interplay of control on different length scales is certainly necessary to develop intricate structures such as diatoms.

REFERENCES AND NOTES

- J. Israelachvili, *Colloids Surf. A* **91**, 1 (1994).
- Q. Huo and G. Stucky, paper presented at the meeting of the Material Research Society, San Francisco, 7 to 11 April 1996.
- C. T. Kresge, M. E. Leonowicz, W. J. Roth, J. C. Vartuli, J. S. Beck, *Nature* **359**, 710 (1992); J. S. Beck *et al.*, *J. Am. Chem. Soc.* **114**, 10834 (1992).
- Q. Huo *et al.*, *Chem. Mater.* **6**, 1176 (1994).
- Q. Huo *et al.*, *Nature* **368**, 317 (1994).
- Q. Huo, R. Leon, P. M. Petroff, G. D. Stucky, *Science* **268**, 1324 (1995).
- Q. Huo, D. I. Margolese, G. D. Stucky, *Chem. Mater.* **8**, 1147 (1996).
- A. Monnier *et al.*, *Science* **261**, 1299 (1993).
- A. Firoúzi *et al.*, *ibid.* **267**, 1138 (1995).
- U. Ciesla *et al.*, *Chem. Commun.* **1994**, 1387 (1994); D. M. Antonelli and J. Y. Ying, *Angew. Chem. Int. Ed. Engl.* **34**, 2014 (1995).
- To date, silica-base synthesis chemistry carried out above the isoelectric point of aqueous solutions of silica has not been successful for the silica composite coating of organic emulsions in water. For organic arrays supported by inorganic substrates [H. Yang, A. Kuperman, N. Coombs, S. Mamiche-Afara, G. A. Ozin, *Nature* **379**, 703 (1996)], surfactants at the air-water interface (G. Ozin, paper presented at the NATO Conference on Supramolecular Chemistry, Montreal, 17 to 20 May 1996), or organic liquid crystals [G. S. Attard, J. C. Glyde, C. G. Goltner, *Nature* **378**, 366 (1995)], only $S^{+}X^{-}$ syntheses at a pH below the aqueous silica isoelectric point have been used.
- The APM samples synthesized below the silica isoelectric point require a counter anion, generally a halide anion, for each surfactant molecule that is present. Terminal Si-O-groups are protonated so that the bulk compositions of M41S and APM materials made with the same surfactant starting materials are distinctly different in hydrogen and halide ion content. The ion-pair surfactants of the APM materials can be readily removed by washing with distilled water at -70°C because the wall charge is neutral or slightly positive. Removal of surfactant from M41S samples requires ion exchange by refluxing with acidic ethanol because of the negatively charged terminal oxygen atoms. The ultimate periodic symmetry is determined in both cases by surfactant packing requirements, so that similar space groups and lattice symmetries are observed by x-ray diffraction and TEM imaging, but with different diffraction intensities. As pointed out by C. J. Brinker and G. W. Scherer [*J. Non-Cryst. Solids* **70**, 301 (1985)], APMs are prepared under conditions that give Huggins or chainlike polymerization, whereas M41S silica polymerization conditions lead to Einstein or clusterlike configurations with extensive cross-linking, so that different silica wall structures are expected. This contrast is evident in nitrogen sorption isotherm measurements, which show that APMs exhibit a sorption behavior different from that of M41S samples, with a step in the isotherm at appreciably lower p/p_0 values (p , pressure) than samples synthesized from alkaline media with a similar lattice spacing. These data and diffraction results show that the APM silica walls are effectively thicker than those of the corresponding M41S phases. Nevertheless, BET surface areas calculated for such samples can be a factor of 2 higher, indicating the presence of micropores or highly ruffled surfaces. Even taking into account the limitations of BET analysis for such materials, the difference in the values obtained indicates a major difference in the pore and wall structure of APM and MCM-41 materials.
- D. Walsh, J. D. Hopwood, S. Mann, *Science* **264**, 1576 (1994).
- The details of the morphology developed during such processes depend not only on the stirring rate but also on the type of stirrer used, the temperature, and the size of the reaction vessel. However, the trends reported in Fig. 1 are the same, although the numerical values of stirring rate to obtain certain morphologies might vary, depending on the other parameters.
- S. Schacht, thesis, Universität Mainz (1995). Such siliceous fibers fall in the classification of potentially carcinogenic fibers and should thus be handled appropriately.
- J. Kärger, private communication; in preparation.
- Concentrations of chlorine in the product correspond to the values reported by Huo *et al.* (6) and are ~ 2 weight %.
- C. M. Zaremba *et al.*, *Chem. Mater.* **8**, 679 (1996); G. Falini, S. Albeck, S. Weiner, L. Addadi, *Science* **271**, 67 (1996).
- This research was supported by the Deutsches Forschungsgemeinschaft (Schu744/12-1), NATO (CRG 950169), NSF (DMR 95-20971, MCB 92-02775), and the Office of Naval Research (N00014-93-10584). We would like to thank S. Schunk, R. Schirach, C. Angelkort, and C. Zaremba for the SEM analyses.

22 April 1996; accepted 5 July 1996

Mongolian Tree Rings and 20th-Century Warming

Gordon C. Jacoby,* Rosanne D. D'Arrigo, Tsevegyn Davaaajamts

A 450-year tree-ring width chronology of Siberian pine (*Pinus sibirica* Du Tour) growing at timberline (2450 meters) in the Tarvagatay Mountains in west central Mongolia shows wide annual growth rings for the recent century. Ecological site observations and comparisons with instrumental temperature records indicate that the ring widths of these trees are sensitive to annual temperature variations. Low-frequency variations in the Tarvagatay tree-ring record are similar to those in a reconstruction of Arctic annual temperatures, which is based on 20 tree-ring width series from northern North America, Scandinavia, and western Russia. The results indicate that recent warming is unusual relative to temperatures of the past 450 years.

Records covering a longer period of time than those that are available from instrumental measurements are essential to evaluation of the causes of climatic change, including possible anthropogenic influences on climate. Three-hundred-year annual temperature reconstructions for the Arctic (1) and Northern Hemisphere (2) based on high-latitude tree-ring data indicate that the warming during the past century seen in instrumental data (3) is unprecedented. However, tree rings usually reflect temperatures during the warm season, and reconstruction of annual temperatures is controversial (4). Records from other areas can complement the high-latitude data. The most appropriate locations are high-elevation tree-line sites where growth is also limited by temperature. During a field investigation in the summer of 1995, we sampled trees growing at timberline in the Tar-

vagatay Mountains of western central Mongolia (Fig. 1). Many trees in Mongolia's forests are old (300 to 500 years) and are undisturbed by human activity.

Mongolia's climate is characterized by extreme continentality (5). It is dominated by the influence of the Siberian (Mongolian) high-pressure cell during the winter (Fig. 1). Rainfall occurs mainly in summer. Mean monthly temperatures in northern Mongolia are -30°C in January to 20°C in July. Daily temperatures range from -50°C to 40°C and can vary by as much as 30°C in 1 day (6).

The northern third of Mongolia is a montane forest-steppe zone (7). At lower elevations, the forests give way to grasslands or to the margins of the Gobi Desert in the south. Forests are most dense on northern shady slopes. In the high western Altai Mountains (Fig. 1), there are permanent snowfields and ice. The tree line is variously formed by Siberian pine (*Pinus sibirica* Du Tour), Siberian larch (*Larix sibirica* Ledebour), or mixed stands of these species. The most prevalent tree species is Siberian larch, with lesser amounts of spruce (*Picea*), pine

G. C. Jacoby and R. D. D'Arrigo, Tree-Ring Laboratory, Lamont-Doherty Earth Observatory, Palisades, NY 10964, USA.

T. Davaaajamts, Institute of Botany, Mongolian Academy of Sciences, Ulaanbaatar 210351, Mongolia.

*To whom correspondence should be addressed.